

High Energy Gain and Transverse Instability in Three-Dimensional Simulations of Light Sail Acceleration

A. Sgattoni,^{1,2,*} S. Sinigardi,^{2,3,4} and A. Macchi^{2,5}

¹*Dipartimento di Energia, Politecnico di Milano, Milano, Italy*

²*Istituto Nazionale di Ottica, Consiglio Nazionale delle Ricerche, research unit “Adriano Gozzini”, Pisa, Italy*

³*Dipartimento di Fisica e Astronomia, Università di Bologna, via Irnerio 46, 40126 Bologna, Italy*

⁴*INFN sezione di Bologna, viale Berti Pichat 6/2, 40127 Bologna, Italy*

⁵*Dipartimento di Fisica “Enrico Fermi”, Università di Pisa, Largo Bruno Pontecorvo 3, I-56127 Pisa, Italy*

(Dated: December 6, 2024)

The dynamics of radiation pressure acceleration in the relativistic light sail regime are analyzed by means of large scale, three-dimensional (3D) particle-in-cell simulations. In 3D the transverse expansion dynamics leads to faster and higher energy gain than in lower dimensionality, in agreement with theoretical predictions. A fast rising Rayleigh-Taylor instability leads to strong transverse modulation of the accelerated ion beam with peculiar structures depending on the pulse polarization and a spatial scale close to the laser wavelength. This latter feature is interpreted on the basis of modulation effects on the radiation pressure.

PACS numbers: 52.38.Kd 41.75.Jv 52.65.Rr 52.35.Py

The development of high power laser systems able to deliver short ultraintense-pulses drove an increasing interest to study laser-plasma interaction with particular focus on realizing compact sources of high energy electrons, ions and photons. In particular, several mechanisms of ion acceleration have been proposed and tested [1] also thanks to progress in target manufacturing [2] and pulse contrast [3]. These latter allowed the first recent experimental investigations of radiation pressure acceleration (RPA) of thin solid foils, i.e. the so-called light sail (LS) regime [4–6]. On the theoretical side, the LS configuration has been proposed and studied in the last ten years and it has been shown through simulations [7] that LS becomes very efficient at intensities beyond $10^{23} \text{ W cm}^{-2}$ (foreseen with next generation facilities) in the regime where the ions become relativistic.

In the basic one-dimensional (1D) picture of LS, the target, provided that its integrity and reflectivity are kept on a sufficiently long time scale, behaves almost as a perfect mirror and can be efficiently accelerated to relativistic velocities $V = \beta c$. The energy gain, though, after an early stage of exponential growth, becomes rather slow [$\gamma(t) \sim t^{1/3}$ where $\gamma = (1 - \beta^2)^{-1/2}$] which would be an issue in a realistic three-dimensional (3D) scenario where the acceleration length required to obtain the maximum energy (for a given laser pulse) may exceed the diffraction length of the laser beam. However, it has been theoretically shown [8] that, in proper conditions and in a multidimensional case where the laser pulse has a finite focal spot, the decrease of the target areal density due to transverse expansion (so that the sail becomes effectively “lighter”) may lead to a faster energy gain, i.e. $\gamma(t) \sim t^{3/5}$ in 3D geometry. A potentially “unlimited” energy gain is thus predicted, although at the expense of the number of accelerated ions.

As an additional issue, the target acceleration may

cause a Rayleigh-Taylor instability (RTI) as observed in 2D simulations [9–12], with some experimental evidence reported in Ref.[5]. The RTI may be a cause of early breakthrough of the laser pulse through the foil and inefficient acceleration.

The RPA-LS regime has been so far investigated extensively with particle-in-cell (PIC) simulations mostly in 1D and 2D (see e.g. Refs.[8, 13]), with few 3D studies having been performed [7, 14–16] mainly because of the very demanding computational requests. Since the scaling of ion energy with time, the diffraction length of the laser beam and the nonlinear RTI evolution are all dependent on the dimensionality, a comprehensive 3D investigation on long time scales is essential. A previous numerical work [14] brought preliminary evidence of ion energies being higher in 3D than in lower dimensionality, but due to limited computing resources the simulations did not reach the end of the acceleration stage.

Here we present the results of large scale 3D simulations performed with the PIC code **ALaDyn** [17]. We followed the LS dynamics in the ultrarelativistic regime until the end of the acceleration stage. We observed that in 3D the energy gain of the fastest ions is higher and faster than in 1D and 2D, and that the evolution of the maximum ion energy with time follows the power laws predicted by the analytical theory of Ref.[8]. The “unlimited” acceleration is however limited by the onset of the target transparency. Peculiar net-like structures in the ion density were observed in the plane perpendicular to the acceleration direction and attributed to the 3D dynamics of a transverse instability. For circular polarization the structure shape resembles that predicted on the general basis of symmetry considerations for RTI. A model accounting for the typical spatial scale of the structure being the laser wavelength is also outlined.

The 3D simulations of Ref.[14] indicated an “oper-

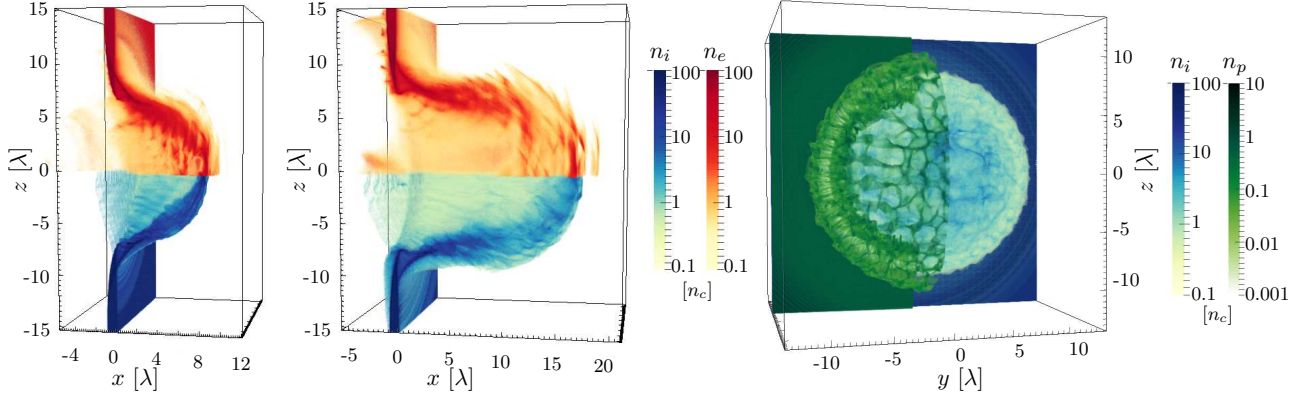


FIG. 1. Left ($t = 20T$) and central ($t = 30T$) panel: 3D snapshots of the density of electrons (red tones, upper half, $z > 0$) and Carbon ions (blue tones, lower half, $z < 0$). Only the $y > 0$ region is shown for visualization purposes. Right panel: snapshot at $t = 30T$ from a different perspective, showing the densities of Carbon ions (for $|y| \leq 15$ and $|z| \leq 15$, blue tones) and of protons (for $-15 \leq y \leq 0$ and $|z| \leq 15$, green tones).

ating point”, defined by the use of circular polarization (CP) of the laser pulse and by the target thickness ℓ_t matching the laser amplitude according to $\zeta = \pi(n_e/n_c)(\ell_t/\lambda) \simeq a_0$ where $a_0 = (I/2m_e c^3 n_c)^{1/2}$, I and λ are the laser intensity and wavelength, respectively, and $n_c = \pi m_e c^2 / e^2 \lambda^2$ is the cut-off density. In these conditions the light sail acceleration was shown to yield the highest ion energy while being relatively unaffected by both limited numerical resolution and inclusion of radiation friction effects. In order to extend the simulations on a much longer time scale we use a lower number of particles per cell after having verified that with such reduction the results of Ref.[14] are unaffected. In addition, we employ a non uniform grid in the transverse direction: a constant cell spacing is maintained in a region around the axis and then gradually stretched (using the tangent as stretching function) towards the edge. This allows us to keep a high resolution in the center and contain the expanding plasma with a reasonable number of grid points. The simulation box is 93λ wide along x (the laser-propagation direction) and 120λ along y and z . In the central region ($93 \times 60 \times 60 \lambda$) the cell size is $\Delta x = \lambda/44$, $\Delta y = \Delta z = \lambda/22$. The grid size is $4096 \times 1792 \times 1792$ cells and 64 macro particles per cell per species are used accounting for a total number of about 2×10^{10} . The simulations were run on 16384 BlueGene/Q cores on FERMI at CINECA (Bologna, Italy).

In the following we mostly focus on a target composed of a first layer of ions with charge to mass ratio $Z/A = 1/2$ (e.g. C^{6+}), thickness $\ell_t = \lambda$ and initial electron density $n_e = 64n_c$, and a second layer of protons, having thickness $\ell_r = \lambda/22$ and density $n_e = 8n_c$. For reasons of computational feasibility, the density is lower than for real solid targets (for comparison Carbon targets have a mean electron density around $400n_c$) but the areal density has a realistic value (for Diamond-like Carbon foils the thickness may be down to $\simeq \lambda/100$). The target configuration mimics a Carbon foil with hydrogen

contaminants on the rear side and allows to differentiate the dynamics of different charge states. The peak normalized amplitude of the laser field corresponding to the “optimal” thickness condition $a_0 \simeq \zeta$ is $a_0 = 198$. In all simulations, the laser pulse has a transverse Gaussian profile with waist diameter $w = 6\lambda$ and a longitudinal \cos^2 -like profile with a FWHM duration $\tau_p = 9T$ (where $T = \lambda/c$ is the laser period), all referred to the profile of the fields. The simulations have been run for a time $t = 80T$, where $t = 0$ corresponds to the moment when the laser pulse front reaches the edge of the target.

Fig.1 shows density snapshots for both electrons and ions at intermediate stages of the acceleration process for a simulation with optimal amplitude $a_0 = 198$. The side view shows the strong typical “cocoon” deformation of the target. The electron density shows structures with longitudinal modulation on the scale of λ , similar to those observed in Refs.[14, 15]. A front view reveals a transverse, net-like structuring of the ion density, which is rather evident in the protons.

First we discuss the ion energy spectra at the end of

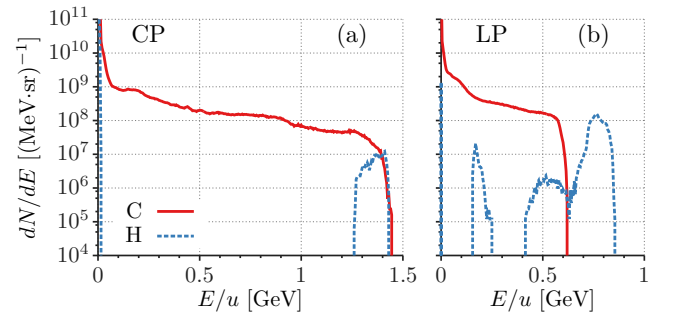


FIG. 2. Energy spectra for carbon ions (solid red line) and protons (dashed blue line) at the end ($t = 80T$) of the simulations with circular (CP, left) and linear (LP, right) polarization, for ions within a cone with semi-aperture 5 of degrees around the x -axis. The absolute numbers in $\text{MeV}^{-1}\text{sr}^{-1}$ have been obtained assuming $\lambda = 0.8\mu\text{m}$.

the simulation of Fig.1. As we are primarily interested in ions moving near the axis we select particles whose momentum is within a cone with a semi aperture of 5 degrees. Inside this cone, the proton spectrum has a narrow peak, while the Carbon distribution is broad as shown in Fig.2 (a). The maximum energy per nucleon of carbon ions and protons are identical indicating that the most energetic particles of both species move at the same velocity. In contrast, for a 3D simulation identical to that of Fig.1 but with linear polarization (LP) instead of CP (and the peak field amplitude $a_0 = 198\sqrt{2} \simeq 280$ to keep the same mean intensity), the ions with different Z/A ratio tend to form separate bands in the energy spectra, with the protons ending up with highest energy and the cut-off for heavier ions being in correspondence of the lower end of the proton peak, as shown in Fig.2 (b). This behavior is also observed in simulations at lower intensity ($a_0 = 100$), both for CP and LP. Similar features were also found experimentally at much lower intensities [6]. Assuming $\lambda = 0.8\mu\text{m}$, we calculated the transverse rms emittance $\epsilon_\perp = (\sigma_\perp \sigma_{p_\perp} - m_\perp^2)^{1/2}$ (being σ_\perp , σ_{p_\perp} , m_\perp respectively the variance of r and of p_\perp and the covariance of (r, p_\perp)) of the ions having energy per nucleon $E > 500\text{MeV/u}$ obtaining 4×10^{-2} and 8×10^{-2} mm mrad for carbon and hydrogen ions, respectively. Such emittance values are compatible with experimental results on laser-driven acceleration at much lower intensities and proton energies [18] (a comparison with values of conventional accelerators is not straightforward due to the non-monochromatic nature of the ion beam).

We now consider the evolution of the cut-off energy of Carbon ions with time, shown in Fig.3 (a). Data for both the 3D simulation of Figs.1-2 and a 2D simulation with the same parameters are shown. In both cases, after an early stage of exponential growth ($t \lesssim 8T$) the time evolution shows an intermediate stage where the time dependence is well fitted by a power law (see below) until the acceleration saturates. Analysis of the simulations shows that such transition occurs when the target becomes transparent to the laser pulse. In the 3D case the energy rises with time faster than in 2D but the transition to transparency is also reached at an earlier time. Eventually the final energy values in 2D and 3D are very close, but both much higher than the 1D value. The cut-off energy of protons from the “contaminant” layer follows the temporal history of the energy of C ions closely.

For the intermediate stage we used a power law $m_p c^2 \gamma(t) = k_D (t - t_0)^{\alpha_D}$ as a fitting function for the energy with three free parameters (k_D , t_0 , α_D). The values of α_D are in very good agreement with the predictions of the analytical model of Ref.[8] in the strongly relativistic, asymptotic limit (see also Ref.[19] for a simplified derivation):

$$\gamma(t) = \left(\frac{t}{\tau_D} \right)^\alpha, \quad \alpha = \frac{D}{D+2} \quad (1)$$

where $D = 1, 2, 3$ is the dimensionality of the system and $\Omega = 2I/\sigma_0 c^2$. The time constants τ_D are

$$\tau_1 = \left(\frac{3}{4\Omega} \right), \quad \tau_2 = \left(\frac{1}{\Omega \bar{\omega}_0} \right)^{1/2}, \quad \tau_3 = \left(\frac{48}{125\Omega \bar{\omega}_0^2} \right)^{1/3}, \quad (2)$$

where the parameter $\bar{\omega}_0$ is the related to the initial transverse momentum $p_\perp = m_p r(0) \bar{\omega}_0$, with $r(0)$ the initial position of the ions. In the model, after an initial “kick”, the ions transverse motion is ballistic with constant momentum p_\perp , and the areal density of the target decreases due to the transverse expansion. An analytical estimate can be obtained considering the effect of the transverse ponderomotive force of a Gaussian laser pulse, $dp_\perp/dt \simeq -m_e c^2 \partial_r \sqrt{1 + \langle a^2(r, t) \rangle}$, where $\langle a^2(r, t) \rangle = a_0^2 \exp(-2r^2/w^2)$. Near the focal axis ($r \ll w$) we have $dp_\perp/dt \simeq m_e c^2 2r/w$ and thus, considering an impulsive acceleration on a time Δt , we obtain $p_\perp \simeq m_e c^2 (2r(0)/w^2) a_0 \Delta t$ and thus

$$\bar{\omega}_0 \simeq 2 \frac{m_e}{m_p} \frac{a_0 c^2 \Delta t}{w^2}. \quad (3)$$

From the fit of Fig.3 $\bar{\omega}_0 \simeq 2.8 \times 10^{-2}$ in the 3D case and $\bar{\omega}_0 \simeq 1.4 \times 10^{-2}$ in 2D. The analytical estimate based on Eq.(3) gives $\bar{\omega}_0 \simeq (2m_e/m_p)(a_0/w^2)\Delta t \simeq 6 \times 10^{-3}(\Delta t/T)$ which matches the simulation result if $\Delta t \simeq 4.7T$.

Simulations were also performed with a slab of hydrogen plasma $Z = A = 1$ as in Refs.[7, 14], all other parameters being equal to Fig. 1. As shown in Fig.3 (c) the energy still follows closely the analytical scaling, reaching higher energies due to the lighter target; the values for the $\bar{\omega}_0$ parameters are 5.5×10^{-2} and 5.7×10^{-2} for the 3D and the 2D case, respectively. However, we notice that in the 2D case the scaling is followed for all the simulation time and the final energy is higher than for the 3D case. For the latter, the extra dimension allows a faster expansion which “boosts” the acceleration, but also leads to an earlier onset of transparency. Looking at the density distribution we observe that the transition to transparency occurs when the peak value is about $10n_c$.

We now discuss the formation of “net-like” structures in the density of ions, both for C ions and for protons, already apparent in Fig.1. In Fig.4 we show the ion areal density on the transverse plane y, z at $t = 60T$, considering only the particles with kinetic energy $E > 300\text{MeV/u}$. For both C^{+6} and H^+ , the net-like pattern is visible; in particular the protons exhibit both a very strong modulation and a denser region in the form of spiral, which is likely to be an imprint of the CP pulse. The simulations for LP also shows a net-like modulation with no spiral and a tendency of the structures to lengthen along the polarization direction. A “synthetic image” (not shown) of both protons and C ions obtained projecting the trajectories of the numerical particles on

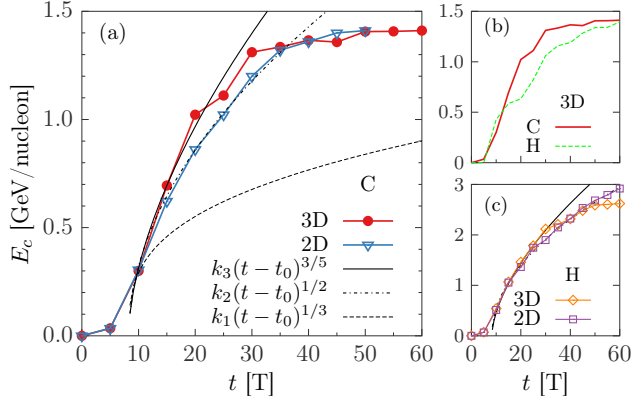


FIG. 3. (a): cut-off energy (GeV) of C ions for the 3D simulation of Fig.1 (red circles) and a 2D simulation with same parameters (blue triangles). The continuous and dash-dotted line represent the fits with power law functions ($k_3 = 220$ and $k_2 = 245$). A similar function with the predicted 1D scaling is drawn for comparison with (dashed line). (b): same as (a), but for a pure hydrogen target ($k_3 = 330$ and $k_2 = 410$). (c) comparison between the energy of C ions and of protons in 3D for the same simulation of (a).

a plane orthogonal to the laser axis, shows very similar features. Such image would correspond to what would be observed, assuming ballistic propagation, on the plane of a detector such as a radiochromic film as in Ref.[5].

The difference in the transverse structures between CP and LP is particularly evident for 3D plane wave simulations, where we took an uniform intensity profile and 5λ as the grid length in y and z . In the CP case we observe a pattern of hexagonal-like structures, which indeed corresponds closely to a theoretical prediction, based on symmetry arguments, for a stable structure of the flow in the nonlinear 3D development of the RTI [20]. It is noticeable that such structure provides an example of spontaneous

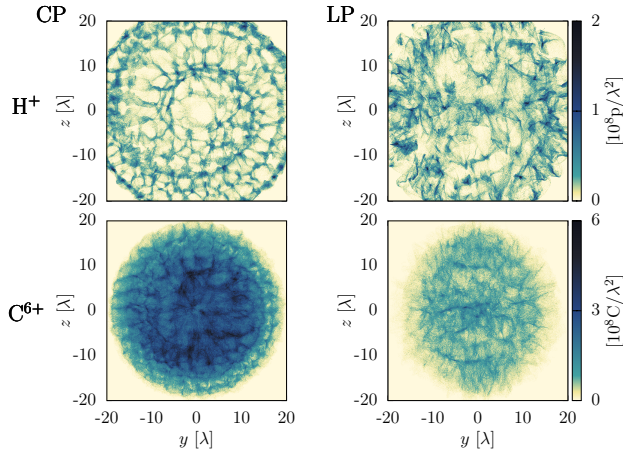


FIG. 4. Areal density of protons (P) and carbon (C) ions having energy $> 300\text{MeV/u}$, obtained by projection of the y, x plane at time $t = 60T$, from the 3D simulation with circular polarization (CP) of Fig.1 and the corresponding simulation with linear polarization (LP).

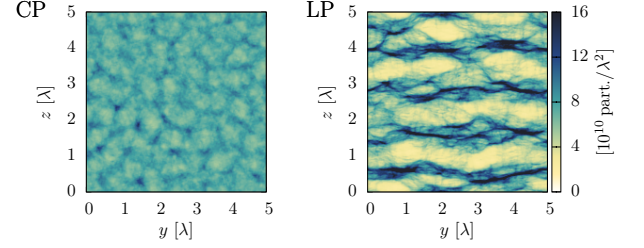


FIG. 5. Areal density of carbon ions at time $t = 15T$ obtained in 3D simulations with same parameters of Fig 4 but for a plane wave, for circular (CP) and linear (LP) polarization.

symmetry breaking in a classical system [21].

For LP, the structures are strongly elongated along the polarization direction, which suggests that the laser transverse electric field “sweeps out” the modulations. For both LP and CP, the transverse structures are visible also in the electron density (not shown) and already at $t \simeq 10T$ (a faster growth being apparent for LP), thus the instability does not prevent to reach relativistic ion energies and to preserve low emittance.

The transverse scale of the instability is close to the laser wavelength λ as it was also observed in several previous simulations in 2D [10–12] (to gain additional confidence that such scale is not affected by “numerical imprinting”, due to the periodicity of either the grid or the domain decomposition in the transverse direction, we performed simulations with some initial temperature and found no difference). Standard hydrodynamical theory as well as specific models oriented to the laser-driven RTI [10, 12] predict a growth rate monotonously increasing with the wavevector q . To understand why the dominant wavevector is $q \simeq k = 2\pi/\lambda$ we consider the possible role of the modulation of the radiation pressure at a rippled interface. Here we summarize the calculation which is presented in detail elsewhere [22]. Assuming a 2D plane geometry we consider the normal incidence (along x) of a monochromatic plane wave on a mirror with a sinusoidally rippled surface (i.e. a grating) described by the curve $x = \delta \cos(qy)/2$. For $q > k$ and in the limit $\delta \ll \lambda$, the radiation pressure at the mirror surface is modulated as $P_{\text{rad}} \simeq (2I/c)[1 + \mathcal{K}(q)\delta \cos(qy)]$ where $\mathcal{K}(q) = (k^2 - q^2/2)(q^2 - k^2)^{-1/2}$ for CP. For $q < k\sqrt{2}$, P_{rad} is stronger in the valleys of the ripple and tends to make it deeper. The strong increase for $q \rightarrow k$ is due to the excitation of a standing surface wave (by the electric field component E_y perpendicular to the grating grooves) in the electromagnetic limit when the grating period equals λ . By inserting the transversely modulated pressure P_{rad} in the model for the thin foil RTI [23], the linear growth rate is modified as

$$\gamma \simeq \gamma_{\text{RT}}(q) \left[\left(1 + \mathcal{K}^2(q)/4q^2 \right)^{1/2} + \mathcal{K}(q)/2q \right]^{1/2}, \quad (4)$$

where $\gamma_{\text{RT}}(q) = (\Omega qc)^{1/2}$ is the well-known result for a non-modulated pressure. Thus, $\gamma = \gamma(q)$ strongly grows

as $q \rightarrow k$, which may explain the observed dominant scale for the RTI. We also notice that for small scales such that $q > 2k$ and not so shallow gratings the field may be screened into the ripple valleys, similarly to what happens in a waveguide.

In conclusion, 3D simulations of light sail acceleration in the relativistic regime show that the energy gain versus time is much faster than in the 1D model and shows a scaling in very good agreement with the analytical theory of Refs.[8]. The energy gain, however, is limited by the onset of target transparency which takes place earlier in 3D than in 2D, counterbalancing the effect of faster rarefaction. The Rayleigh-Taylor instability of the target has been characterized in 3D showing for CP the formation of peculiar shapes predicted by theory, and which can be detected easily in experiments by looking at the transverse structures of the ion beam. The role of radiation pressure modulations in modifying the unstable wavevector spectrum has been discussed. These findings are highly relevant to the design of next generation facilities for laser-driven ion acceleration at ultra-relativistic intensity.

We are grateful to F. Pegoraro for enlightening discussions and to P. Londrillo for help with the ALaDyn code. We acknowledge PRACE for access to the Blue-Gene/Q “FERMI”, based in Italy at CINECA, via the project “LSAIL”. Support from MIUR, Italy, via the FIR project “SULDIS” is also acknowledged.

* andrea.sgattoni@polimi.it

- [1] H. Daido, M. Nishiuchi, and A. S. Pirozhkov, Rep. Prog. Phys. **75**, 056401 (2012); A. Macchi, M. Borghesi, and M. Passoni, Rev. Mod. Phys. **85**, 751 (2013).
- [2] W. Ma, V. Liechtenstein, J. Szerypo, D. Jung, P. Hilz, B. Hegelich, H. Maier, J. Schreiber, and D. Habs, Nucl. Inst. Meth. Phys. Res. A **655**, 53 (2011).
- [3] B. Dromey, S. Kar, M. Zepf, and P. Foster, Rev. Sci. Instrum. **75**, 645 (2004); C. Thauray *et al.*, Nat. Phys. **3**, 424 (2007).
- [4] A. Henig *et al.*, Phys. Rev. Lett. **103**, 245003 (2009); F. Dollar *et al.*, *ibid.* **108**, 175005 (2012); I. J. Kim *et al.*, *ibid.* **111**, 165003 (2013); B. Aurand *et al.*, New J. Phys. **15**, 033031 (2013); S. Steinke *et al.*, Phys. Rev. ST Accel. Beams **16**, 011303 (2013).
- [5] C. A. J. Palmer *et al.*, Phys. Rev. Lett. **108**, 225002 (2012).
- [6] S. Kar *et al.*, Phys. Rev. Lett. **109**, 185006 (2012).
- [7] T. Esirkepov, M. Borghesi, S. V. Bulanov, G. Mourou, and T. Tajima, Phys. Rev. Lett. **92**, 175003 (2004).
- [8] S. V. Bulanov *et al.*, Phys. Rev. Lett. **104**, 135003 (2010); S. V. Bulanov, E. Y. Echkina, T. Z. Esirkepov, I. N. Inovenkov, M. Kando, F. Pegoraro, and G. Korn, Phys. Plasmas **17**, 063102 (2010).
- [9] S. C. Wilks, W. L. Kruer, M. Tabak, and A. B. Langdon, Phys. Rev. Lett. **69**, 1383 (1992).
- [10] F. Pegoraro and S. V. Bulanov, Phys. Rev. Lett. **99**, 065002 (2007).
- [11] M. Chen, N. Kumar, A. Pukhov, and T.-P. Yu, Phys. Plasmas **18**, 073106 (2011).
- [12] V. Khudik, S. A. Yi, C. Siemon, and G. Shvets, Phys. Plasmas **21**, 013110 (2014).
- [13] O. Klimo, J. Psikal, J. Limpouch, and V. T. Tikhonchuk, Phys. Rev. ST Accel. Beams **11**, 031301 (2008); A. P. L. Robinson, M. Zepf, S. Kar, R. G. Evans, and C. Bellei, New J. Phys. **10**, 013021 (2008); A. Macchi, S. Veghini, T. V. Liseykina, and F. Pegoraro, *ibid.* **12**, 045013 (2010); X. Q. Yan, H. C. Wu, Z. M. Sheng, J. E. Chen, and J. Meyer-ter-Vehn, Phys. Rev. Lett. **103**, 135001 (2009); B. Qiao, M. Zepf, M. Borghesi, B. Dromey, M. Geissler, A. Karmakar, and P. Gibbon, *ibid.* **105**, 155002 (2010).
- [14] M. Tamburini, T. V. Liseykina, F. Pegoraro, and A. Macchi, Phys. Rev. E **85**, 016407 (2012).
- [15] T.-P. Yu, A. Pukhov, Z.-M. Sheng, F. Liu, and G. Shvets, Phys. Rev. Lett. **110**, 045001 (2013).
- [16] H. Xu *et al.*, Appl. Phys. Lett. **104**, 024105 (2014).
- [17] C. Benedetti, A. Sgattoni, G. Turchetti, and P. Londrillo, IEEE Trans. Plasma Science **36**, 1790 (2008); P. Londrillo, C. Benedetti, A. Sgattoni, and G. Turchetti, Nucl. Inst. Meth. Phys. Res. A **620**, 28 (2010).
- [18] T. E. Cowan *et al.*, Phys. Rev. Lett. **92**, 204801 (2004); F. Nuernberg *et al.*, Rev. Sci. Instrum. **80**, 033301 (2009).
- [19] A. Macchi, arXiv:1403.6273 [physics.plasm-ph].
- [20] S. I. Abarzhi, Phys. Rev. E **59**, 1729 (1999).
- [21] L. Michel, Rev. Mod. Phys. **52**, 617 (1980).
- [22] A. Macchi, A. Sgattoni, and F. Pegoraro, arXiv:1404.1260 [physics.plasm-ph].
- [23] E. Ott, Phys. Rev. Lett. **29**, 1429 (1972).